Lagrangian Supersaturation Fluctuations at the Cloud Edge

Lagrangian Supersaturation Fluctuations at the Cloud Edge

J. Fries,[1] G. Sardina,[2] G. Svensson,[3,4] A. Pumir,[5] and B. Mehlig[1]
[1]Department of Physics, Gothenburg University, SE-41296 Gothenburg, Sweden
[2]Department of Mechanics and Maritime Sciences, Chalmers University of Technology, 41296 Gothenburg, Sweden
[3]Department of Meteorology and Bolin Centre for Climate Research, Stockholm University, SE-106 91 Stockholm, Sweden
[4]Department of Engineering Mechanics, KTH Royal Institute of Technology, SE-114 28 Stockholm, Sweden
[5]Université Lyon, ENS de Lyon, Université Claude Bernard, CNRS, Laboratoire de Physique, F-69342, Lyon, France

(Received 6 September 2023; accepted 6 November 2023; published 18 December 2023)

Evaporation of cloud droplets accelerates when turbulence mixes dry air into the cloud, affecting droplet-size distributions in atmospheric clouds, combustion sprays, and jets of exhaled droplets. The challenge is to model local correlations between droplet numbers, sizes, and supersaturation, which determine supersaturation fluctuations along droplet paths (*Lagrangian* fluctuations). We derived a statistical model that accounts for these correlations. Its predictions are in quantitative agreement with results of direct numerical simulations, and explain the key mechanisms at play.

DOI: 10.1103/PhysRevLett.131.254201

Introduction.—When dry air is mixed into a cloud, water droplets at the cloud edge evaporate. This causes the droplet-size distribution to broaden [1], affecting the radiative properties of the cloud [2], and is also a prerequisite for rain formation [3]. Droplet evaporation occurs in many other contexts too, e.g., in combustion [4–8], ocean sprays [9], and for respiratory droplets in exhaled jets of air [10–14]. In these systems, an essential physical ingredient is that evaporating droplets saturate the surrounding air. But the subtle coupling between phase change and turbulent mixing at widely separated turbulent scales [15] makes it difficult to predict the local supersaturation and, as a consequence, droplet-size distributions. In this work, we study the interplay between these processes and their influence on droplet growth, focusing on the parameter regime relevant to the edge of a cloud.

The distribution of supersaturation at droplet positions—the Lagrangian distribution—can be strongly non-Gaussian. Direct numerical simulations (DNS) of transient mixing of a three-dimensional slab of cloudy air with the surrounding dry air [Fig. 1(a)] show exponential tails [16–19]. Non-Gaussian supersaturation fluctuations are also seen in cloud-chamber experiments [20–22]. Without phase change, a passive scalar field mixed by turbulence can exhibit non-Gaussian concentration fluctuations in the presence of a mean scalar gradient [23–25]. Without the mean gradient, however, the steady-state distribution is essentially Gaussian [17,18,26,27]. Non-Gaussian tails may appear in transient mixing [28], but must eventually disappear in a homogeneous system.

Whether the tail of the Lagrangian supersaturation distribution is Gaussian or not makes a significant difference, because the tail determines how rapidly certain droplets evaporate, and thereby influences the sizes of the remaining droplets, and thus the droplet-size distribution in unknown ways.

The key question is thus how droplet phase change affects the Lagrangian supersaturation distribution. When phase change is frequent and rapid, no consideration of

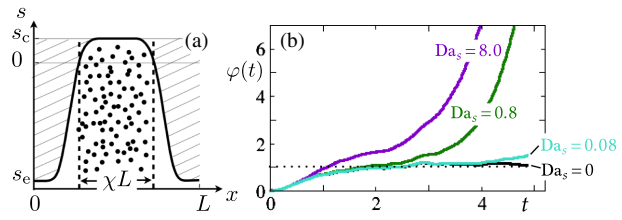

FIG. 1. (a) Initial condition used in Refs. [16–19,29]: a three-dimensional slab of cloudy air with supersaturation $s_c \geq 0$, containing droplets (filled black circles) with initial number density n_0, surrounded by dry subsaturated air with $s_e < 0$ (hashed). The supersaturation profile is shown as a solid line. The cloudy air occupies a volume fraction χ. (b) Statistical-model rate $\varphi(t)$ as a function of time for different Damköhler numbers; see Eq. (4) and SM [30] for details. Parameters: $\chi = 0.4$, $\mathrm{Da_s} = 0.08$, $\mathrm{Da_d} = 0.0073$; $\mathrm{Da_s} = 0.80$, $\mathrm{Da_d} = 0.073$; $\mathrm{Da_s} = 8.0$, $\mathrm{Da_d} = 0.73$ (solid lines). Parameters from Ref. [17], but the value of τ_L in our DNS differs slightly from that in Ref. [17] due to statistical variability in the forcing. The dotted line is the steady-state limit $\varphi_* = C_\phi/2$ for a passive scalar with $C_\phi = 2$ [34] (see text).

passive-scalar mixing can explain the non-Gaussian relaxation of the Lagrangian supersaturation distribution. Large-eddy simulations of droplet growth by condensation in a cloud chamber [21] show an anticorrelation between supersaturation $s(\boldsymbol{x},t)$ and the local droplet-number density $n(\boldsymbol{x},t)$ in the steady state: in regions with many droplets, the air is strongly subsaturated (very negative values of s), while it is less so in regions with few droplets (less negative s). It is plausible that this effect may change the tails of the Lagrangian supersaturation distribution, but existing stochastic models [29,35–41] cannot explain this, because they do not describe how $s(\boldsymbol{x},t)$ is affected by phase change locally.

We derived a statistical model that describes transient Lagrangian supersaturation fluctuations developing from an initial inhomogeneity, such as the configuration shown in Fig. 1(a), and performed DNS for this configuration to validate the model. We show here that the model captures the key mechanisms that determine the shape of the Lagrangian supersaturation distribution. First, when mixing occurs on timescales much shorter than phase change, non-Gaussian tails form only during the initial transient, and large-time relaxation is characterized by a Gaussian distribution of $s(\boldsymbol{x},t)$. Second, in the opposite limit of rapid phase change, the distribution is no longer Gaussian. Strong phase change drives the mean of the distribution close to its upper bound, while the variance decays more slowly. The distribution is squeezed and becomes non-Gaussian. This is reflected in a strong positive correlation between n and s, formed because phase change tends to establish saturation in regions with many droplets. This mechanism—the opposite of the effect described in Ref. [21]—explains the tails in the Lagrangian supersaturation distribution described in earlier studies [16–19]. Beyond this qualitative explanation, the model predicts supersaturation distributions in excellent quantitative agreement with DNS results. The key to success is that the model inherits its supersaturation dynamics from first principles, rather than imposing an external driving resulting in a Gaussian steady state [35,36,39].

We start from simplified microscopic equations [29] governing droplet evaporation in turbulent flow:

$$\partial_t \boldsymbol{u} + (\boldsymbol{u}\cdot\boldsymbol{\nabla})\boldsymbol{u} = -\varrho_\mathrm{a}^{-1}\boldsymbol{\nabla}p + \nu\nabla^2\boldsymbol{u}, \qquad \boldsymbol{\nabla}\cdot\boldsymbol{u} = 0, \tag{1a}$$

$$\partial_t s + (\boldsymbol{u}\cdot\boldsymbol{\nabla})s = \kappa\nabla^2 s - A_2 C_d, \tag{1b}$$

$$\frac{\mathrm{d}}{\mathrm{d}t}\boldsymbol{x} = \boldsymbol{u}, \qquad \frac{\mathrm{d}}{\mathrm{d}t}r = A_3 s/r. \tag{1c}$$

Equation (1a) is the Navier-Stokes equation for the incompressible fluid-velocity field $\boldsymbol{u}(\boldsymbol{x},t)$, where ϱ_a is the mass density of air, and ν its kinematic viscosity. Equation (1b) describes supersaturation $s = q_\mathrm{v}/q_\mathrm{vs} - 1$, with water-vapor mixing ratio $q_\mathrm{v} = \varrho_\mathrm{v}/\varrho_\mathrm{a}$, the ratio of the mass densities of vapor and air, and κ is the diffusivity of supersaturation. Further, $C_d(\boldsymbol{x},t) = (4\pi/3)\varrho_\mathrm{w} n(\boldsymbol{x},t)\overline{(\mathrm{d}/\mathrm{d}t)r^3}$ is the local rate of change of droplet mass, averaged over all droplets in the vicinity of $\boldsymbol{x}$ with droplet radius r. Here ϱ_w is the liquid-water density, and $n(\boldsymbol{x},t)$ is the droplet-number density. Equations (1c) state that the droplets follow the flow, and how the droplet radius r changes [42].

We emphasize that the dynamics (1) is transient and tends towards a well-mixed steady state. The variance $\sigma_s^2(t)$ of supersaturation fluctuations tends to zero due to dissipation (with scalar dissipation rate $\varepsilon_s \equiv 2\kappa\langle|\boldsymbol{\nabla}s|^2\rangle$) and phase change:

$$\frac{\mathrm{d}}{\mathrm{d}t}\sigma_s^2 = -\varepsilon_s - 2A_2(\langle sC_d\rangle - \langle s\rangle\langle C_d\rangle). \tag{2}$$

Here, the averages are over a given microscopic configuration at time t.

How the steady state is approached depends on the nondimensional parameters of the problem. We nondimensionalize Eqs. (1) and (2) as follows [29]: time, velocities, and positions with the large-eddy turnover time $\tau_L = k/\varepsilon$ (with turbulent kinetic energy k and kinetic dissipation rate ε), and the turbulent rms velocity $u_0 = \sqrt{2k/3}$; supersaturation with $|s_\mathrm{e}|$, where s_e is the initial subsaturation of the dry air outside the cloud; droplet radii with the initial average droplet radius r_0. In the limit of large Reynolds number, the following nondimensional parameters remain: the Damköhler numbers $\mathrm{Da_d} = \tau_L/\tau_\mathrm{d}$ and $\mathrm{Da_s} = \tau_L/\tau_\mathrm{s}$ (with supersaturation relaxation time τ_s and droplet-evaporation time τ_d defined as in [29]), and the volume fraction χ of cloudy air [Fig. 1(a)]. The Schmidt number $\mathrm{Sc} = \nu/\kappa$ is of order unity [43].

Earlier attempts to analyze the process were based on statistical models of mixing and evaporation that describe droplet evaporating in direct response to a spatially inhomogeneous mean field given by an ensemble average, $\langle s(\boldsymbol{x},t)\rangle$ [40,41,44]. A more sophisticated model [29] accounts for how droplet-phase change is affected by Lagrangian supersaturation fluctuations, but still assumes that they decay exponentially towards the mean. Both types of models explain how the extent of complete droplet evaporation depends on the Damköhler numbers, but fail to reproduce the far tail of cloud-droplet-size distribution obtained in DNS [16–19]. A likely reason is that these models underestimate the magnitude of supersaturation fluctuations. A further shortcoming is that these models assume exponential relaxation of supersaturation to $\langle s(\boldsymbol{x},t)\rangle$. As a consequence, they fail to reproduce the passive-scalar limit [34], namely Gaussian supersaturation fluctuations with exponentially decaying variance.

The question of how a passive-scalar distribution relaxes as it is mixed by turbulence has a long history. Eswaran and Pope [45] analyzed this process systematically using DNS.

Their results inspired and benchmarked increasingly accurate models for passive-scalar mixing [28,46–51].

Model.—The mapping-closure approximation [50,51] describes how the shape of a passive-scalar distribution changes as the scalar is mixed in turbulence. The approximation relies only on one-point statistics. Correlations are not needed. As a consequence, the approximation does not predict the speed of the mixing process, but yields accurate and robust predictions for the sequence of shapes of the distribution. Therefore it is ideally suited for our purposes. The mapping closure for *Eulerian* supersaturation fluctuations starts from

$$s(\boldsymbol{x},t) = X\{\xi[\boldsymbol{x}/\lambda(t)],t\}, \tag{3}$$

where $\lambda(t)$ is a time-dependent length scale, ξ is a spatially smooth random Gaussian field with mean zero and unit variance, and X is the time-dependent mapping from $\xi[\boldsymbol{x}/\lambda(t)]$ to $s(\boldsymbol{x},t)$. Inserting (3) into (1b), one obtains

$$\partial_t X = \varphi(t)(-\eta\partial_\eta X + \partial_\eta^2 X) - \mathrm{Da_s}\langle C_d|s=X\rangle. \tag{4}$$

In comparison to the original model [50,51], Eq. (4) contains the phase-change term $\langle C_d|s=X\rangle = X\langle rN/V|s=X\rangle$, with droplet number N and spatial volume V. We approximate this term by a mean-field decoupling of the conditional average [see Supplemental Material (SM) [30] for details]

$$\langle C_d|s=X\rangle = X\langle r|s=X\rangle\langle N|s=X\rangle/\langle V|s=X\rangle. \tag{5}$$

The factor $\varphi(t) = \kappa/[u_0^2\tau_L\lambda^2(t)]$ in Eq. (4) is the nondimensional relaxation rate of the Eulerian distribution. How $\varphi(t)$ changes as a function of time is determined by processes at both small and large length scales, as the following argument shows. For passive-scalar mixing, the scalar variance decays exponentially in the self-similar regime [34], $(\mathrm{d}/\mathrm{d}t)\sigma_s^2 = -C_\phi\sigma_s^2$. with $C_\phi \approx 2$. In this case, $\varphi(t)$ approaches the steady-state value, $\varphi_* \sim C_\phi/2$. The steady state emerges as a balance between the scalar variance cascading toward large wave numbers and rapid dissipation at large wave numbers. In physical dimensions, the steady-state length scale $\lambda_* = [2\kappa k/(C_\phi\varepsilon)]^{1/2}$ equals $\lambda_\mathrm{T}(5C_\phi\mathrm{Sc})^{-1/2}$ where $\lambda_\mathrm{T} = (10\nu k/\varepsilon)^{1/2}$ is the Taylor microscale. In other words, both large-scale mixing and small-scale diffusion matter.

With phase change, $\varphi(t)$ is unknown. We determine it using DNS; see (SM) [30] for details. The results are summarized in Fig. 1(b) which shows how $\varphi(t)$ evolves as a function of t. For passive-scalar mixing, the predicted plateau at φ_* is approached after two large-eddy turnover times, at $t \approx 2$. With phase change, $\varphi(t)$ is larger, corresponding to smaller $\lambda(t)$. This is consistent with the notion that phase change generates supersaturation gradients by driving the air toward saturation where droplets exist, while subsaturated regions without droplets remain subsaturated.

To obtain the Lagrangian supersaturation fluctuations, Pope [51] suggested to use a Langevin equation for $\xi(t)\mathrm{d}\xi = -R(t)\xi\mathrm{d}t + [2R(t)]^{\frac{1}{2}}\mathrm{d}v$, where $\mathrm{d}v$ is the increment of a Gaussian random process, and to compute the supersaturation as $s(t) = X[\xi(t),t]$. The Langevin equation ensures that the distribution of $\xi(t)$ relaxes to a normalized Gaussian, and the function $X(\eta,t)$ maps this Gaussian to the Eulerian supersaturation distribution. This ensures that the Lagrangian supersaturation distribution relaxes to the Eulerian one, as required. We set $R(t) = C\varphi(t)$, where C is a constant. This is motivated—at least for a passive scalar—by the fact that supersaturation fluctuations due to turbulent mixing experienced by a fluid element reflect the diffusive term $\kappa\nabla^2 s$ in Eq. (1b), and that the fluctuations of this term are proportional to $\varphi(t)$ under the mapping closure. Comparison with DNS shows that $R(t) = C\varphi(t)$ works very well for the first two large-eddy turnover times, for $\mathrm{Da_s}$ up to 8.0. We find that C decreases as $\mathrm{Da_s}$ increases (see SM [30]), because phase change tends to maintain saturation in regions with droplets. For times much larger than the large-eddy turnover time, the precise form of $R(t)$ does not matter because the Lagrangian distribution has almost relaxed to the Eulerian one.

Results.—Figure 2 shows the Lagrangian supersaturation distribution $P_\mathrm{L}(s;t)$ from the statistical model, solid lines, compared with DNS results (see SM [30] for details), symbols. Shown are two cases: small and large Damköhler numbers (parameters from Ref. [17]). We see that the model reproduces the DNS results quantitatively.

For small $\mathrm{Da_s}$, the effect of phase change is small at short times; the distribution is close to that of a passive scalar (blue dashed line). Supersaturation behaves essentially like a passive scalar during the first large-eddy turnover time,

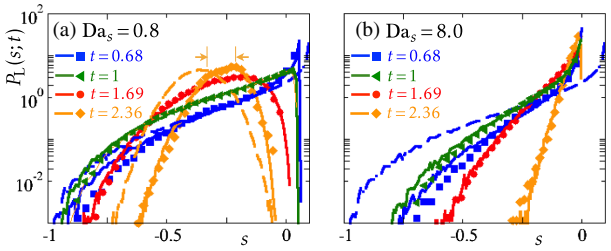

FIG. 2. Lagrangian supersaturation distributions. (a) $\mathrm{Da_s} = 0.80$, $\mathrm{Da_d} = 0.073$, $\chi = 0.4$ (parameters from Ref. [17]). DNS results (see SM [30] for details): symbols ($t = 0.68$, blue filled square; $t = 1$, green filled triangle; $t = 1.69$, red filled circle; $t = 2.36$, orange filled diamond). Statistical-model simulations: solid lines. Statistical-model simulations for a passive scalar ($t = 0.68$, 2.36, dashed). The shift due to phase change is indicated by horizontal arrows. (b) Same as (a) but for $\mathrm{Da_s} = 8.0$, $\mathrm{Da_d} = 0.73$ [17]; passive-scalar result shown only for $t = 0.68$. The DNS results were obtained using the same turbulent velocity field and the same initial conditions.

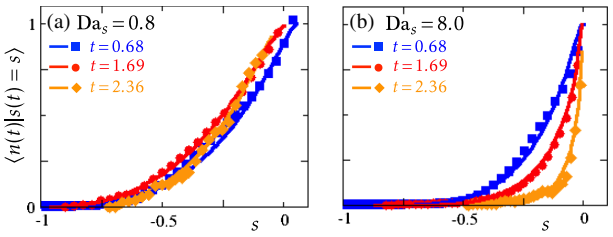

FIG. 3. Correlations between droplet-number density and supersaturation. Average $\langle n(t)|s(t) = s\rangle$ of droplet-number density at time t conditional on local supersaturation s. (a) $\mathrm{Da_s} = 0.80$, $\mathrm{Da_d} = 0.073$, and $\chi = 0.4$ (parameters from Ref. [17]). DNS results (see SM [30] for details): symbols ($t = 0.68$, blue filled square; $t = 1.69$, red filled circle; $t = 2.36$, orange filled diamond). Statistical-model simulations (lines). (b) Same as (a) but for $\mathrm{Da_s} = 8.0$ and $\mathrm{Da_d} = 0.73$ [17].

$t \sim 1$. At later times, droplet-phase change matters more, but its effect is straightforward, it causes the peak of the distribution to shift somewhat compared to the distribution for $\mathrm{Da_s} = 0$ (orange dashed line), to less negative values of s, while supersaturation fluctuations are still approximately Gaussian [Fig. 2(a)]. For larger values of $\mathrm{Da_s}$, by contrast, the evolution of the supersaturation distributions looks very different [Fig. 2(b)]. The distribution remains non-Gaussian at large times.

To pin down the precise mechanism, we followed the droplet-number density $n(t)$ and the local supersaturation $s(t)$ for different fluid parcels in DNS. The results are summarized in Fig. 3 which shows the conditional average of the local-droplet number density conditional on the surrounding supersaturation for the same parameters as in Fig. 2. For small Damköhler numbers, the average does not change much during the time shown; it is still strongly influenced by the initial condition. For large $\mathrm{Da_s}$, by contrast, the average changes rapidly, and the positive correlation between $n(t)$ and $s(t)$ increases significantly. The statistical model captures this very well. The mechanism is simply that a parcel containing many droplets cannot remain sub- or supersaturated for long, because phase change drives the air quickly towards saturation when $\mathrm{Da_s}$ is large. As a consequence, parcels with few droplets tend to have much more negative values of s, compared with a parcel with small $\mathrm{Da_s}$. The strong suppression of the conditional average $\langle n(t)|s(t) = s\rangle$ at large $\mathrm{Da_s}$ explains how the non-Gaussian tails evolve in Fig. 2(b): the left tail of $P_\mathrm{L}(s;t)$ disappears quickly as time increases, because droplets saturate their surroundings, and therefore fewer of them experience very dry air.

For small $\mathrm{Da_s}$, the mapping closure results in Gaussian relaxation. Phase change causes non-Gaussian tails. In order to describe these tails, it is necessary to condition C_d on supersaturation, Eq. (5). The conditioning also ensures that the supersaturation fluctuations remain bounded, as they must because neither phase change nor mixing can turn subsaturated into supersaturated air.

Discussion.—We begin by discussing in more detail, how our results relate passive-scalar mixing. Eswaran and Pope [45] described the shape change of the Eulerian passive-scalar distribution as a function of time. The initial condition [Fig. 1(a)] dictates that the Eulerian distribution is, initially, the sum of two narrow peaks, located at $s = s_\mathrm{c}$ and s_e. It relaxes first to a U-shaped form. The left tail of the Lagrangian supersaturation distribution reflects how the Eulerian peak at $s = s_\mathrm{c}$ broadens. At large times, the Eulerian U-shaped distribution relaxes to a Gaussian.

Our model predicts the same for small but not negligible $\mathrm{Da_s}$, with one important difference: phase change causes the mean of the Lagrangian supersaturation distribution to shift to the right [Fig. 2(a)], while mixing causes the distribution to narrow, remaining approximately Gaussian. In this case, the mapping is approximately given by $X(\eta, t) = \sigma_s(t)\eta + \mu_s(t)$. Inserting this into Eq. (4) and assuming passive-scalar relaxation of the width, $\mathrm{d}\sigma_s/\mathrm{d}t = -C_\phi\sigma_s/2$, yields $\mathrm{d}\mu_s/\mathrm{d}t = -\mathrm{Da_s}\mu_s$. So the standard deviation decays more rapidly than the mean for small $\mathrm{Da_s}$, consistent with Gaussian relaxation.

At large $\mathrm{Da_s}$, the time evolution of the Lagrangian supersaturation distribution is strongly affected by phase change, resulting in persistent non-Gaussian tails [Fig. 2(b)]. Our model explains why the Lagrangian supersaturation distributions relax so differently for small and large $\mathrm{Da_s}$. Rapid phase change quickly drives the mean of the distribution toward the upper bound of the supersaturation distribution. As a result, the distribution is squeezed toward $s = 0$, thus preventing a Gaussian from forming. The distribution is bounded because subsaturated air cannot obtain a positive supersaturation through droplet evaporation. Therefore saturation ($s = 0$) constitutes an upper bound for the Lagrangian supersaturation fluctuations.

We contrast our results with those of Prabhakaran *et al.* [21]. They found a negative correlation between $n(t)$ and $s(t)$ in large-eddy simulations designed to model droplet condensation in a cloud chamber. Their system is statistically stationary, but the statistical model highlights the mechanism leading to their findings. In their case, the air is saturated or supersaturated, so droplets tend to grow by condensation. The resulting drive towards saturation gives rise to a negative correlation between $n(t)$ and $s(t)$.

The model describes not only the Lagrangian supersaturation fluctuations quantitatively, but also the droplet-size distribution (not shown, see SM [30]). Our earlier model [29] yielded qualitative but not quantitative agreement, highlighting the importance of correlations between n and s.

We recall that Damköhler numbers in atmospheric clouds tend to be large, simply because the relevant length scale L is large, causing large τ_L. It is tempting to argue that the persistent left tail of the Lagrangian supersaturation distribution at large Damköhler numbers in Fig. 2(b) is

more representative of atmospheric relaxation than the Gaussian relaxation at small Damköhler numbers. However, the local supersaturation field around individual droplets is difficult to observe *in situ*. Observations resolving supersaturation at larger scales, of the order of one meter, indicate Gaussian distributions [52], but better resolved laboratory measurements reveal skewed distributions [53], as predicted by our model.

Here we analyzed moist systems, with $\mathrm{Da_d}/\mathrm{Da_s} \propto (\rho_w n_0 r_0^3)^{-1} \sim 0.1$. We expect the present model to apply equally well to dry clouds where complete droplet evaporation occurs frequently, but we have not yet explored this regime.

Villermaux *et al.* [7] measured the joint dynamics of vapor and droplets in a dense acetone spray. They analyzed vapor concentrations for different flow configurations considering the limit of large droplet-number density n_0 and large Damköhler numbers, where the droplets in the spray prevent each other from evaporating, but evaporate instantaneously in dry air. In this limit, correlations between $n(\boldsymbol{x}, t)$ and $s(\boldsymbol{x}, t)$ are extreme, and it remains to be seem whether they can be captured by our model. More generally, it is of interest to compare the accuracy of the present mapping-closure model with predictions of the linear-eddy model [54], where turbulent stretching and folding is represented by a one-dimensional map [55–57].

Conclusions.—We derived a statistical model for the transient supersaturation fluctuations around droplets near the cloud edge, where turbulence mixes dry with cloudy air, causing the droplets to evaporate. The model explains the key mechanisms determining Lagrangian supersaturation fluctuations, and its predictions are in quantitative agreement with earlier DNS studies of droplet evaporation at the cloud edge [16–19,29]. This advance became possible because the model describes supersaturation dynamics and the local coupling due to phase change using a mapping closure, which is known to yield quantitative results for passive-scalar mixing. At the same time, the model is simple enough so that it can be used to resolve subgrid scale effects in large-eddy simulations with high precision.

We stress that the present model, unlike earlier statistical models, accounts for local correlations between droplet numbers and supersaturation. This opens the possibility to model the dynamics of denser turbulent aerosols, such as industrial sprays.

A. P. and B. M. thank E. Bodenschatz for numerous discussions on the subject. J. F. was supported by grants from the Knut and Alice Wallenberg Foundation (No. 2014.0048) and Vetenskapsrådet (VR), Grant No. 2021-4452. G. Sardina acknowledges support from VR (Grant No. 2022-03939). The computations were enabled by resources provided by the National Academic Infrastructure for Supercomputing in Sweden and the Swedish National Infrastructure for Computing at the National Supercomputer Centre and the Parallel-datorcentrum, partially funded by VR through Grant Agreements No. 2022-06725 and No. 2018-05973. The collaboration of A. P. and B. M. during the *Multiphase 22* program at the K. I. T. P. was supported in part by the National Science Foundation under Grant No. NSF PHY-1748958.

[1] M. J. Beals, J. P. Fugal, R. A. Shaw, J. Lu, S. M. Spuler, and J. L. Stith, Holographic measurements of inhomogeneous cloud mixing at the centimeter scale, Science **350**, 87 (2015).
[2] A. Kokhanovsky, Optical properties of terrestrial clouds, Earth Sci. Rev. **64**, 189 (2004).
[3] W. W. Grabowski and L. P. Wang, Growth of cloud droplets in a turbulent environment, Annu. Rev. Fluid Mech. **45**, 293 (2013).
[4] M. Sommerfeld and H. H. Qiu, Experimental studies of spray evaporation in turbulent flow, Int. J. Heat Fluid Flow **19**, 10 (1998).
[5] W. A. Sirignano, Advances in droplet array combustion theory and modeling, Prog. Energy Combust. Sci. **42**, 54 (2014).
[6] Patrick Jenny, Dirk Roekaerts, and Nijso Beishuizen, Modeling of turbulent dilute spray combustion, Prog. Energy Combust. Sci. **38**, 846 (2012).
[7] E. Villermaux, A. Moutte, M. Amielh, and P. Meunier, Fine structure of the vapor field in evaporating dense sprays, Phys. Rev. Fluids **2**, 074501 (2017).
[8] F. Dalla Barba and F. Picano, Clustering and entrainment effects on the evaporation of dilute droplets in a turbulent jet, Phys. Rev. Fluids **3**, 034304 (2018).
[9] F. Veron, Ocean spray, Annu. Rev. Fluid Mech. **47**, 507 (2015).
[10] W. F. Wells, On air-borne infection: Study II. Droplets and droplet nuclei, Am. J. Epidemiol. **20**, 611 (1934).
[11] R. Mittal, Rand Ni, and J. H. Seo, The flow physics of COVID-19, J. Fluid Mech. **894**, F2 (2020).
[12] J. Wang, F. Dalla Barba, A. Roccon, G. Sardina, A. Soldati, and F. Picano, Modelling the direct virus exposure risk associated with respiratory events, J. R. Soc. Interface **19**, 20210819 (2022).
[13] K. L. Chong, C. S. Ng, N. Hori, R. Yang, R. Verzicco, and D. Lohse, Extended lifetime of respiratory droplets in a turbulent vapor puff and its implications on airborne disease transmission, Phys. Rev. Lett. **126**, 034502 (2021).
[14] G. Bagheri, O. Schlenczek, L. Turco, B. Thiede, K. Stieger, J. M. Kosub, S. Clauberg, M. L. Pöhlker, J. Molácek C. Pöhlker, S. Scheithauer, and E. Bodenschatz, Size, concentration, and origin of human exhaled particles and their dependence on human factors with implications on infection transmission, J. Aerosol Sci. **168**, 106102 (2023).
[15] E. Bodenschatz, S. P. Malinowski, R. A. Shaw, and F. Stratmann, Can we understand clouds without turbulence?, Science **327**, 970 (2010).

[16] B. Kumar, J. Schumacher, and R. A. Shaw, Cloud microphysical effects of turbulent mixing and entrainment, Theor. Comput. Fluid Dyn. **27**, 361 (2013).
[17] B. Kumar, F. Janetzko, J. Schumacher, and R. A. Shaw, Extreme responses of a coupled scalar-particle system during turbulent mixing, New J. Phys. **14**, 115020 (2012).
[18] B. Kumar, J. Schumacher, and R. A. Shaw, Lagrangian mixing dynamics at the cloudy-clear air interface, J. Atmos. Sci. **71**, 2564 (2014).
[19] B. Kumar, P. Götzfried, N. Suresh, J. Schumacher, and R. A. Shaw, Scale dependence of cloud microphysical response to turbulent entrainment and mixing, J. Adv. Model. Earth Syst. **10**, 2777 (2018).
[20] S. Thomas, P. Prabhakaran, W. Cantrell, and R. A. Shaw, Is the water vapor supersaturation distribution Gaussian?, J. Atmos. Sci. **78**, 2385 (2021).
[21] P. Prabhakaran, S. Thomas, W. Cantrell, R. A. Shaw, and F. Yang, Sources of stochasticity in the growth of cloud droplets: Supersaturation fluctuations versus turbulent transport, J. Atmos. Sci. **79**, 3145 (2022).
[22] T. MacMillan, R. A. Shaw, W. H. Cantrell, and D. H. Richter, Direct numerical simulation of turbulence and microphysics in the Pi Chamber, Phys. Rev. Fluids **7**, 020501 (2022).
[23] A. Pumir, B. Shraiman, and E. D. Siggia, Exponential tails and random advection, Phys. Rev. Lett. **66**, 2984 (1991).
[24] Jayesh and Z. Warhaft, Probability distribution of a passive scalar in grid-generated turbulence, Phys. Rev. Lett. **67**, 3503 (1991).
[25] J. P. Gollub, J. Clarke, M. Gharib, B. Lane, and O. N. Mesquite, Fluctuations and transport in a stirred fluid with a mean gradient, Phys. Rev. Lett. **67**, 3507 (1991).
[26] Jayesh and Z. Warhaft, Probability distribution, conditional dissipation, and transport of passive temperature fluctuations in grid-generated turbulence, Phys. Fluids A **4**, 2292 (1992).
[27] Z. Warhaft, Passive scalars in turbulent flows, Annu. Rev. Fluid Mech. **32**, 203 (2000).
[28] E. Villermaux, Mixing vs stirring, Annu. Rev. Fluid Mech. **51**, 256 (2019).
[29] J. Fries, G. Sardina, G. Svensson, and B. Mehlig, Key parameters for droplet evaporation and mixing at the cloud edge, Q. J. R. Meteorol. Soc. **147**, 2160 (2021).
[30] See Supplemental Material at http://link.aps.org/supplemental/10.1103/PhysRevLett.131.254201 for details regarding the numerical computations. It also contains Refs. [31–33].
[31] G. Sardina, S. Poulain, L. Brandt, and R. Caballero, Broadening of cloud droplet size spectra by stochastic condensation: Effects of mean updraft velocity and CCN activation, J. Atmos. Sci. **75**, 451 (2018).
[32] J. Fries, Mixing and evaporation at the cloud edge and angular dynamics of small crystals in viscous flow, Ph.D. thesis, University of Gothenburg, 2022.
[33] S. Bi, M. Broggi, and M. Beer, The role of the Bhattacharyya distance in stochastic model updating, Mech. Syst. Signal Process. **117**, 437 (2019).
[34] S. B. Pope, *Turbulent Flows* (Cambridge University Press, Cambridge, England, 2000).
[35] G. Sardina, F. Picano, L. Brandt, and R. Caballero, Continuous growth of droplet size variance due to condensation in turbulent clouds, Phys. Rev. Lett. **115**, 184501 (2015).
[36] R. Paoli and K. Shariff, Turbulent condensation of droplets: Direct simulation and a stochastic model, J. Atmos. Sci. **66**, 723 (2009).
[37] C. Siewert, J. Bec, and G. Krstulovic, Statistical steady state in turbulent droplet condensation, J. Fluid Mech. **810**, 254 (2017).
[38] K. K. Chandrakar, W. Cantrell, K. Chang, D. Ciochetto, D. Niedermeier, M. Ovchinnikov, R. A. Shaw, and F. Yang, Aerosol indirect effect from turbulence-induced broadening of cloud-droplet size distributions, Proc. Natl. Acad. Sci. U.S.A. **113**, 14243 (2016).
[39] G. C. Abade, W. W. Grabowski, and H. Pawlowska, Broadening of cloud droplet spectra through eddy hopping: Turbulent entraining parcel simulations, J. Atmos. Sci. **75**, 3365 (2017).
[40] M. Pinsky, A. Khain, and A. Korolev, Theoretical analysis of mixing in liquid clouds—Part 3: Inhomogeneous mixing, Atmos. Chem. Phys. **16**, 9273 (2016).
[41] C. A. Jeffery, Inhomogeneous cloud evaporation, invariance, and Damköhler number, J. Geophys. Res. **112**, D24S21 (2007).
[42] R. Rogers and M. Yau, *A Short Course in Cloud Physics* ((Pergamon, New York, 1989).
[43] P. A. Vaillancourt, M. K. Yau, and W. W. Grabowski, Microscopic approach to cloud droplet growth by condensation. Part I: Model description and results without turbulence, J. Atmos. Sci. **58**, 1945 (2001).
[44] M. Pinsky and A. Khain, Analytical investigation of the role of lateral mixing in the evolution of nonprecipitating cumulus. Part I: Developing clouds, J. Atmos. Sci. **77**, 891 (2020).
[45] V. Eswaran and S. B. Pope, Direct numerical simulations of the turbulent mixing of a passive scalar, Phys. Fluids **31**, 506 (1988).
[46] L. Valino and C. Dopazo, A binomial Langevin model for turbulent mixing, Phys. Fluids A **3**, 3034 (1991).
[47] R. O. Fox, The Fokker–Planck closure for turbulent molecular mixing: Passive scalars, Phys. Fluids A **4**, 1230 (1992).
[48] R. O. Fox, The spectral relaxation model of the scalar dissipation rate in homogeneous turbulence, Phys. Fluids **7**, 1082 (1995).
[49] D. W. Meyer and P. Jenny, A mixing model for turbulent flows based on parameterized scalar profiles, Phys. Fluids **18**, 035105 (2006).
[50] H. Chen, S. Chen, and R. H. Kraichnan, Probability distribution of a stochastically advected scalar field, Phys. Rev. Lett. **63**, 2657 (1989).
[51] S. B. Pope, Mapping closures for turbulent mixing and reaction, Theor. Comput. Fluid Dyn. **2**, 255 (1991).
[52] H. Siebert and R. A. Shaw, Supersaturation fluctuations during the early stage of cumulus formation, J. Atmos. Sci. **74**, 975 (2017).
[53] J. C. Anderson, S. Thomas, P. Prabhakaran, R. A. Shaw, and W. Cantrell, Effects of the large-scale circulation on temperature and water vapor distributions in the Pi Chamber, Atmos. Meas. Tech. Discuss. **14**, 5473 (2021).

[54] A. R. Kerstein, A linear-eddy model of turbulent scalar transport and mixing, Combust. Sci. Technol. **60**, 391 (1988).
[55] S. K. Krueger, Linear eddy modeling of entrainment and mixing in stratus clouds, J. Atmos. Sci. **50**, 3078 (1993).
[56] C. W. Su, S. K. Krueger, P. A. McMurtry, and P. H. Austin, Linear eddy modeling of droplet spectral evolution during entrainment and mixing in cumulus clouds, Atmos. Res. **47–48**, 41 (1998).
[57] F. Hoffmann, T. Yamaguchi, and G. Feingold, Inhomogeneous mixing in Lagrangian cloud models: Effects on the production of precipitation embryos, J. Atmos. Sci. **76**, 113 (2019).